LIMNOLOGY
AND
OCEANOGRAPHY

January 1998
Volume 43
Number 1

Limnol. Oceanogr., 43(1), 1998, 1–9

Bioturbation and porosity gradients

Sandor Mulsow[1] *and Bernard P. Boudreau*[2]
Department of Oceanography, Dalhousie University, Halifax, Nova Scotia B3H 4J1

John N. Smith
DFO Canada, Bedford Institute of Oceanography, P.O. Box 1006, Dartmouth, Nova Scotia B2Y 4A2

Abstract

Ubiquitous porosity gradients have a potentially important effect on the mixing of particle-bound tracers, such as ^{210}Pb. Mass-depth coordinates cannot be used to deal with these effects if values of the traditional mixing coefficient, D_B, are required. This paper compares and evaluates three different means of dealing directly with porosity gradients while modeling bioturbation, i.e. mean constant porosity, interphase mixing (porosity mixed), and intraphase mixing (porosity not mixed). We apply these models to 11 different ^{210}Pb profiles collected at various depths and times on the eastern Canadian Margin. A statistical analysis of the resulting best fits shows that these models produce equivalent mixing coefficient values for 55% of the profiles. For the remaining 45% of the profiles, the interphase mixing model predicts the existence of well-mixed near-surface zones on the time scale of ^{210}Pb decay, a phenomenon not predicted by the other models. Unfortunately, our tracer dataset by itself cannot be used to establish which mixing mode is actually operative at each station.

Virtually all fine-grained sediments exhibit appreciable decreases in porosity, φ, with depth due to compaction (Berner 1980). If the overlying waters are oxic, these sediments are also subject to bioturbation. Porosity modification has also been ascribed to the actions of bioturbators (e.g. Rhoads 1974; Rhoads and Boyer 1982; McCall and Tevesz 1982). Macrofauna can increase the porosity at depth by egesting bulk sediment (i.e. solids plus associated water that was ingested nearer to the sediment surface), by injecting water during burrowing (Rhoads and Boyer 1982), and by manipulating and vertically displacing pieces of bulk sediment with their appendages. However, it is also possible to envision both ingestion and displacement of particles that would leave the water behind while moving the solids.

Bioturbation also redistributes the various components of solid sediments, often in what appears to be a diffusive manner. The intensity of this biodiffusion can be determined from the depth distribution of natural and manmade tracers in the upper decimeters of sediments (Guinasso and Schink 1975; Berner 1980).

How bioturbation alters porosity and how macrofauna mix solid tracers in sediments are related questions. Two end-member relationships between tracer bioturbation and porosity modification exist. The first possibility is that bioturbation acts to decrease porosity gradients by diffusively mixing the volume fraction occupied by pore water against that occupied by solids at the same rate as tracers are mixed; therefore, in a sediment accumulating at steady state, the porosity gradient would be weaker than in an equivalent nonmixed compacting sediment. If the pore water is called the fluid phase and the total solids the solid phase of a sediment, then the phases are intermixed by the bioturbation in this scenario; for this reason, it can be called interphase mixing (Boudreau 1986).

The other end-member possibility is that bioturbation does not modify porosity, contrary to the ascertions given above, and that it only acts to decrease gradients of solid species, leaving the porosity distribution unchanged. A steady-state porosity profile/gradient would then result from accumulation and compaction acting alone, independent of the bio-

[1] Present address: Akvaplan SA, Strandtarget 2B, P.O. Box 735, N-9001 Tromso, Norway.
[2] Corresponding author.

Acknowledgments

This research was supported by the CJGOFS CSP grant from the Natural Sciences and Research Council of Canada. Our sincere gratitude goes out to all our colleagues in the CJGOFS Benthic Processes Study who participated in the cruises during which we obtained our data: B. Sundby, A. Mucci, G. Desrosiers, N. Silverberg, R. Marinelli, A. Hatcher, J. Grant, D. Webb, K. Juniper, T. Arakaki and S. Zhong. We also thank David DeMaster and a second anonymous reviewer for their comments, as well as David Kirchman for a reality check.

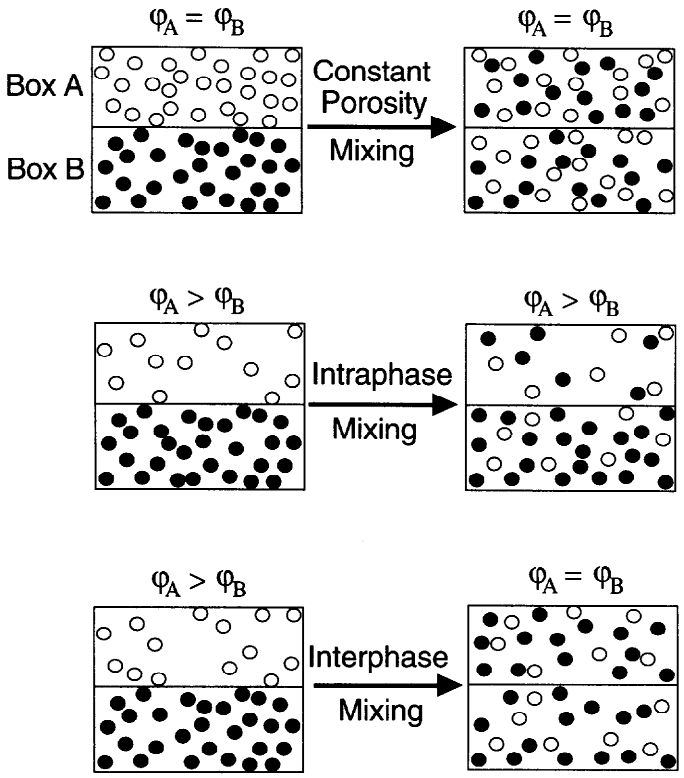

Fig. 1. Schematic representation of transient mixing of a nonreactive tracer (color) between two boxes by the three possible modes studied in this paper. The top diagram illustrates the conventional case of mixing with *constant porosity,* i.e. surface box and bottom boxes have the same porosity, $\varphi_A = \varphi_B$, but the particles in the surface box A are all white, while those beneath in box B are all black. After complete mixing, the boxes have the same number of white and black particles. The middle diagram illustrates *intraphase mixing.* In this case, the porosities and the number of each type of particle are initially different between the two boxes, but after complete mixing only the particle distributions have been homogenized; the porosity is not mixed and its distribution unaltered, i.e. $\varphi_A > \varphi_B$. Finally, the bottom diagram illustrates *interphase mixing.* The starting situation is identical to intraphase mixing, but this time both porosity and particle-type differences are eliminated by complete mixing.

turbation. The two phases, solids and fluid, do not intermix in this case, and tracer biodiffusion is dependent only on its own gradient in the solid phase; for this reason, this situation can be called intraphase mixing (Boudreau 1986). The spectrum between the stated end-member mixing models allows for mixing of porosity, but at a progressively slower rate than a solid tracer, until the limit of intraphase mixing is reached. Bioturbation in real sediments lies undoubtedly somewhere within this spectrum.

These two end-member possibilities are not, however, the only *modi operandi* assumed by modellers when considering porosity gradients and bioturbation. By far the most common (but perhaps ostrichlike) strategy is to adopt a constant mean value for the porosity and ignore its depth dependence. This has the merit of mathematical simplicity, but at what price?

To help further understand the difference between these possible modes of bioturbation, it is worthwhile to consider the hypothetical experiment depicted in Fig. 1. Three treatments are presented in this figure—each consists of two boxes of sediment that are in contact with each other but are closed to the outside world. The sediment consists of a number of colored beads, with only black beads in the bottom box and white in the top box at the beginning of each experiment. These beads do not decay or change color (i.e. they are stable tracers). The initial porosity, φ, is also prescibed in each case. Hypothetical diffusive bioturbators are introduced at the begining of each experiment, and the distribution of both bead color and porosity is determined after sufficient time to obtain a steady state.

The top treatment illustrates what happens when porosity is constant or is assumed to be so. After a long time, the number of white and black beads is the same in each box, and the porosity is equal and the same as in the begining. The middle boxes depict what happens during intraphase mixing. Here, there is a porosity difference initially, as well as bimodal distribution of bead colors. After mixing is complete, there is no gradient in bead color, but the porosity difference remains unaffected. Finally, the bottom experiment displays the effects of interphase mixing. Porosity and bead-color differences (gradients) initially exist, but both are obliterated by the end of the experiment. The discussion that follows deals with steady-state diagenesis, yet the transient situations depicted in Fig. 1 do highlight the essential differences in the mixing models.

It is our aim to determine if the choice of mixing mode (i.e. constant porosity, interphase or intraphase mixing) leads

Notation

B	Activity of a tracer (dpm g^{-1})
D_B	Biodiffusion coefficient with assumed constant porosity (cm^2 yr^{-1})
D_B*	Biodiffusion coefficient with interphase mixing (cm^2 yr^{-1})
$D_B^\bullet$	Biodiffusion coefficient with intraphase mixing (cm^2 yr^{-1})
E	Mass-depth biodiffusion coefficient (g^2 cm^{-4} yr^{-1})
F_B	Bioturbational flux of tracer with constant porosity (dpm cm^{-2} yr^{-1})
F_B*	Bioturbational flux of tracer with interphase mixing (dpm cm^{-2} yr^{-1})
$F_B^\bullet$	Bioturbational flux of tracer intraphase mixing (dpm cm^{-2} yr^{-1})
t	Time (yr)
U	Mass-depth burial velocity (g cm^2 yr^{-1})
w	Burial velocity of solids with constant porosity mixing or intraphase mixing (cm yr^{-1})
w*	Burial velocity of solids with interphase mixing (cm yr^{-1})
x	Depth relative to the sediment–water interface (cm)
z	Mass depth as defined by Eq. 8 (g cm^{-2})
α	Attenuation constant (free parameter) in Eq. 10 (cm^{-1})
φ	Porosity (cm^3 pore water cm^{-3} bulk)
φ_s	Solid volume fraction, $1 - \varphi$ (cm^3 solid cm^{-3} bulk)
$\varphi_s(0)$	Solid volume fraction at the sediment–water interface ($x = 0$)
$\varphi_s(\infty)$	Asymptotic solid volume fraction at great depth ($x \rightarrow \infty$)
λ	First-order decay constant (yr^{-1})

to serious differences in calculated mixing rates and if natural ^{210}Pb distributions are better described by one or another of these models. We already know that a disagreement with regard to these types of mixing has been at the heart of one serious debate in the scientific literature (i.e. Christensen 1983 vs. Officer and Lynch 1983).

Description of models

For constant porosity mixing, the diffusive flux of a solid species, F_B, is given by (Berner 1980)

$$F_B = -\varphi_s D_B \frac{\partial B}{\partial x}, \tag{1}$$

where x is depth relative to the sediment–water interface (cm), B is the activity or concentration of the solid species or tracer (dpm cm^{-3}), D_B is the biodiffusion coefficient for constant porosity mixing (cm^2 yr^{-1}), and φ_s is the solid volume fraction, $1 - \varphi$, where φ is the porosity. Because φ_s is a constant, its value will affect the absolute magnitude of the flux only by limiting the area for that flux, but it will not affect the shape of the solid species profile. The depth distribution of a radioactive tracer is then governed by the familiar equation

$$\frac{\partial B}{\partial t} = \frac{\partial}{\partial x}\left(D_B \frac{\partial B}{\partial x} - wB\right) - \lambda B, \tag{2}$$

where t is time, w is the burial velocity, and λ is the decay constant.

For interphase mixing, the diffusive flux, F_B*, is (e.g. Nozaki et al. 1977; Aller et al. 1980; Christensen 1982)

$$F_B^* = -D_B^* \frac{\partial \varphi_s B}{\partial x}, \tag{3}$$

where D_B* is the biodiffusion coefficient for interphase mixing (cm^2 yr^{-1}). With Eq. 3, the conservation equation for a simple radioactive tracer would be

$$\frac{\partial \varphi_s B}{\partial t} = \frac{\partial}{\partial x}\left(D_B^* \frac{\partial \varphi_s B}{\partial x} - w^* \varphi_s B\right) - \lambda \varphi_s B, \tag{4}$$

where w* is the apparent burial velocity (Boudreau 1986) with interphase mixing. Notice that φ_s and B always appear as the product $\varphi_s B$ in this last equation; therefore, by simply defining a new dependent variable, $B^* = \varphi_s B$, Eq. 4 is transformed into the more familiar form (Krishnaswami et al. 1980)

$$\frac{\partial B^*}{\partial t} = \frac{\partial}{\partial x}\left(D_B^* \frac{\partial B^*}{\partial x} - w^* B^*\right) - \lambda B^*. \tag{5}$$

Depth profiles of B can be obtained from the solutions for B* by dividing by a known $\varphi_s(x)$.

The flux, $F_B^\bullet$, for intraphase mixing for a solid species is given by (e.g. Officer and Lynch 1982; Cochran 1985)

$$F_B^\bullet = -\varphi_s D_B^\bullet \frac{\partial B}{\partial x}, \tag{6}$$

where $D_B^\bullet$ is the biodiffusion coefficient for intraphase mixing (cm^2 yr^{-1}). The corresponding conservation equation for a tracer is

$$\frac{\partial \varphi_s B}{\partial t} = \frac{\partial}{\partial x}\left(\varphi_s D_B^\bullet \frac{\partial B}{\partial x} - w\varphi_s B\right) - \lambda \varphi_s B, \tag{7}$$

where w is the burial velocity in the absence of mixing. To facilitate solution of Eq. 7, Officer and Lynch (1982) introduced the so-called mass-depth transformation, z, i.e.

$$z = \int_0^x \rho_s(1 - \varphi)\, dx = \int_0^x \rho_s \varphi_s\, dx, \tag{8}$$

where ρ_s is the density of the dry solids. Substitution into Eq. 7 obtains the more familiar form

$$\frac{\partial B}{\partial t} = \frac{\partial}{\partial z}\left\{E \frac{\partial B}{\partial z} - UB\right\} - \lambda B, \tag{9}$$

where $U \equiv \rho_s(1 - \varphi)w = \rho_s \varphi_s w$ and $E \equiv [\rho_s(1 - \varphi)]^2 D_B^\bullet = (\rho_s \varphi_s)^2 D_B^\bullet]$. E has units of g^2 cm^{-4} yr^{-1}, and U has units of g cm^{-2} yr^{-1}.

If E and U can be treated as constants, then Eq. 9 is again the standard diffusion-decay equation with its known solutions. Officer and Lynch (1982) then stated that E can be translated into a $D_B^\bullet$ value by using a mean value of φ. In actuality, this procedure will not produce a correct result because φ_s is the controlling variable in defining E and not φ. Changes in φ are typically modest in the bioturbated zone of sediments, e.g. from 0.9 to 0.7 (Andrews and Hargrave 1984; Archer et al. 1989; Iversen and Jørgensen 1993); conversely, the corresponding changes in φ_s are large indeed, i.e. a factor of 2–3. Thus, while the mean porosity is reasonably representative of the weakly varying porosity, the mean of φ_s is a quite poor representative of this function. In addition, the definition of E given above squares φ_s, making the approximation even worse. The conversion of E into a constant $D_B^\bullet$ value is *not justifiable* under typical sedimentary conditions. The same is true of a conversion between U and w.

In the remainder of this paper, we first determine if an interphase or an intraphase mixing model provides a better explanation of observed ^{210}Pb distributions in bioturbated sediments with porosity gradients. Second, we determine if there is an effective difference in the D_B values predicted by these models, and if these values are significantly different from that obtained by a constant porosity model. To meet these stated goals, we compare model fits to observed distributions of porosity and ^{210}Pb from the five Canadian JGOFS sites on the Atlantic Margin and in the Gulf of Saint Lawrence.

Methods

Sites and sampling—Sediment cores were collected from five stations located in the lower part of the Gulf of Saint Lawrence (Fig. 2, Sta. 1, 2, and 3) and from the continental shelf off Nova Scotia (Fig. 2, Sta. 4 and 5) on the eastern coast of Canada. These stations were visited at least twice (Sta. 1, 2, and 3; winter 1993, summer 1994), Sta. 4 was

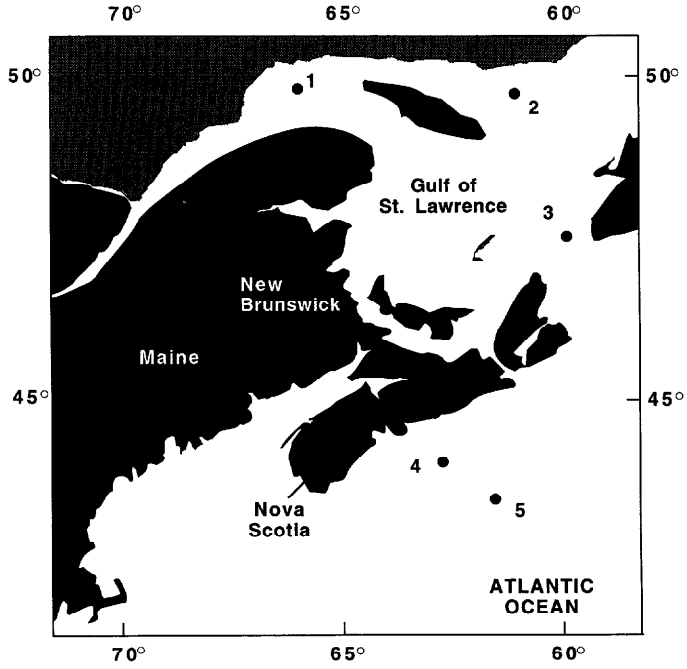

Fig. 2. A map of eastern Canada that shows the locations of the five Canadian JGOFS stations. (For information on water depth contours in this area, *see* figs. 4 and 5 in Keen et al. 1971.)

sampled three times (summer + winter 1993, summer 1994), and Sta. 5 in summer 1993 and 1994. These stations represent a reasonably wide range of water depths (230–820 m, Table 1). Because of ship drift during coring and errors in positioning, repeated samples at any given station can be as much as 1 km apart.

Sediment samples were collected using a multicore at all stations, with the exception of Sta. 4 and 5 on the first cruise (summer 1993), which were obtained by subsampling a box core with Plexiglas tubes of same dimension as those used in the multicore. Cores were sliced every half centimeter from the surface to 1 cm, and thereafter every 1 cm when possible (i.e. no cracks present).

Porosity—At each interval, a subsample of sediment was collected to determine bulk density from the difference between wet and dry (105°C for 48 h) weights. The porosity was calculated assuming a dry solids density of 2.45 g cm^{-3}, which is the average for marine sediments around Nova Scotia. A salt correction was applied based on the bottom salinity (Table 1).

^{210}Pb—Sediment for radiogenic analyses was kept at 4°C during transportation and was subsequently freeze-dried and homogenized. ^{210}Pb was determined by isotope dilution analysis and alpha counting of both ^{210}Po and ^{208}Po (the latter for efficiency calculations) after electro-deposition onto nickel disks. The ^{226}Ra-supported ^{210}Pb was determined on acid-digested samples by using a radon gas-emanation technique (Mathieu et al. 1988); specifically, 1–2 g of sediment was dissolved in a mixture of 1 ml octano, 10 ml nitric acid, 10 ml hydrofluoric acid that was heated in a Teflon bomb for 90 s in a microwave oven. The ^{226}Ra was measured only on the deepest samples in each core. All samples were counted until errors were <5% of the activity of samples.

Table 1. Basic site and bottom water properties at the eastern Canadian JGOFS sites at each sampling time.

Sta.	Sampling date	Water depth (m)	Temp. (°C)	Salinity
1	5–15 Dec 93	331	5.07	34.3
1	19 Jun 94	360	5.18	34.4
2	5–15 Dec 93	262	4.78	34.0
2	21 Jun 94	245	5.12	34.4
3	5–15 Dec 93	494	5.36	34.6
3	21 Jun 94	531	5.32	34.7
4	8 May 93	232	9.40	34.8
4	5–15 Dec 93	230	9.86	34.7
4	28 Jun 94	230	10.24	35.1
5	10 May 93	816	6.1	34.9
5	27 Jun 94	830	5.0	34.9

Regression methods—Regressions, both linear and nonlinear, for the constant porosity and interphase mixing models were done with the built-in regression functions in the computer program Kaleidagraph for the Apple Macintosh computer. Regressions for the intraphase mixing model were done with Fortran routines from the ACM-approved Minpack package.

Results and discussion

Solid volume fraction—Figure 3 displays the φ_s data collected at our sampling sites. The measurements are generally quite regular, except for Sta. 2 in summer 1994, which probably represents a small burrow or recent bioturbation event. The changes in φ_s with depth are no less than a factor of two at any station, and they are as great as a factor of three at Sta. 1 in summer 1994. These results argue that φ_s cannot be well represented by a simple mean value; instead, we fit this data with an empirical formula of the form

$$\varphi_s(x) = \varphi_s(\infty) - \left[\varphi_s(\infty) - \varphi_s(0)\right]e^{-\alpha x}, \qquad (10)$$

where $\varphi_s(0)$ and $\varphi_s(\infty)$ are the values at the interface and at great depth, respectively, and α is an attenuation coefficient (cm^{-1}). All three of these quantities act as fitting parameters. The resulting best-fit values are presented in Table 2. The values of the coefficient of determination, R^2, show that Eq. 10 accounts for ≥90% of the variance in these data; consequently, it is a good representation of these type of data, and it can be used in conjunction with the solution to the mixing models to produce ^{210}Pb-activity profiles.

Excess ^{210}Pb—The main aim of the following discussion is to evaluate the merits of the three possible mixing models, i.e. assumed constant porosity, interphase mixing, and intraphase mixing. To evaluate both the constant porosity and intraphase mixing models, our ^{210}Pb data are plotted first in log-linear form in Fig. 4 for all stations. On the other hand, the counting errors are not re-displayed in Fig. 5, which is used for the interphase mixing model, as the errors in this

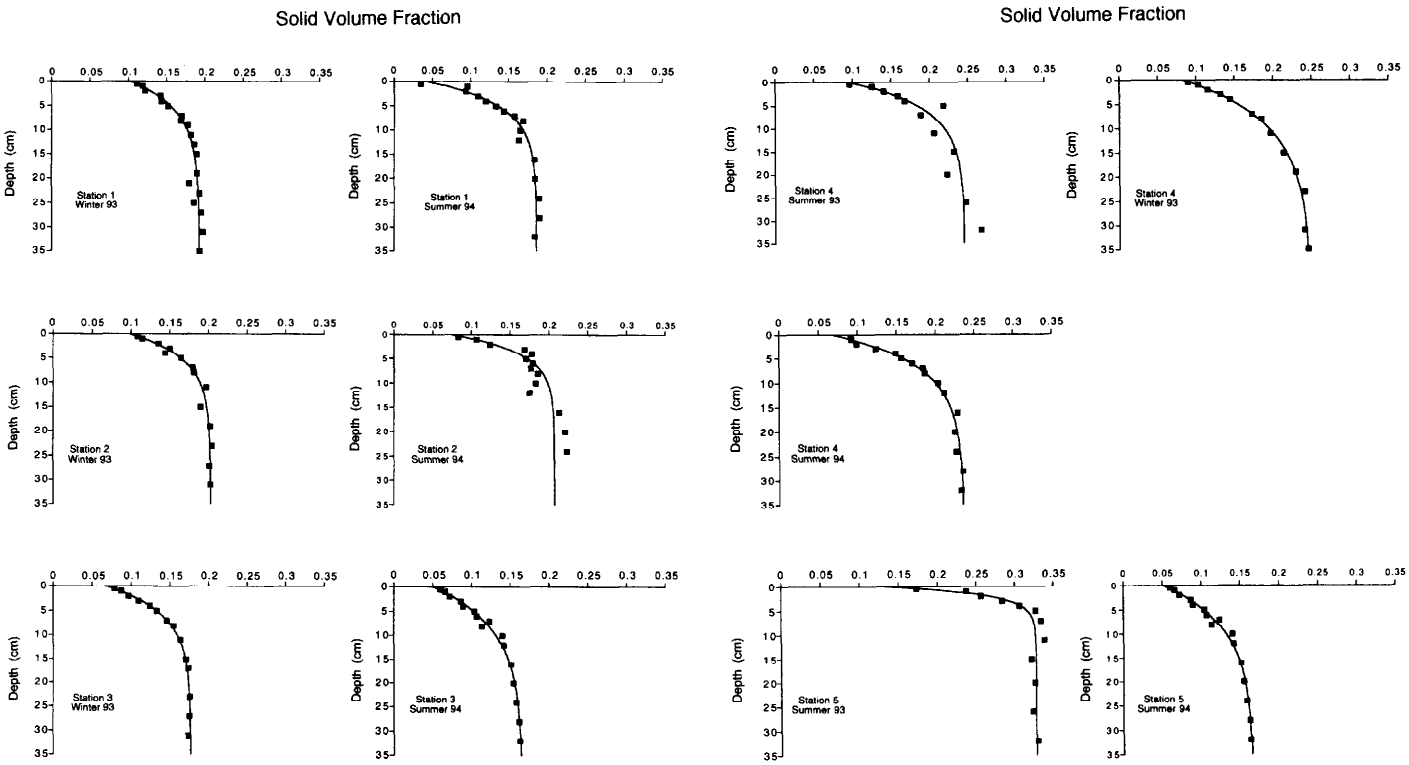

Fig. 3. Plots of solid volume fraction, $1 - \varphi$, changes with depth in the upper few decimeters of sediments collected at the stations illustrated in Fig. 2 during three cruises. The solid lines are best fits with Eq. 10 of the text, and the corresponding parameters values can be found in Table 2.

figure should include the error on the solid volume fraction determination, which we do not know. In addition, the sampling intervals are not shown in either figure as errors because these play no role in the analyses.

In applying any of the models, we have assumed steady-state diagenesis and negligible burial relative to mixing. In comparing the winter 1993 and summer 1994 data at Sta. 1, 2 and 3, there is a suggestion of temporal changes, either seasonal or related to a depositional event; however, there is much that argues against either interpretation.

First, the calculated mixing coefficients are too small to accommodate seasonal changes in the ^{210}Pb that would be implied by these distributions, as proven further below. Additionally, temperature and the rate of O_2 consumption are apparently not seasonally variable (unpubl. CJGOFS data).

Second, we do not think that the summer 1994 profiles reflect the rapid deposition of as much as 5 cm of sediment during the intervening period. The St. Lawrence River system does not constitute a reasonable source for the required amount of sediment and slump or turbidite deposition at our widely dispersed sites would require an unusual and unrecorded mechanism. The temporal differences could be due to some unknown or unappreciated sampling artifact, but simultaneously acquired solute profiles of O_2, NO_3^- and ΣCO_2 display no anomalies (unpubl. CJGOFS data). More likely, the differences are simply due to spatial heterogeneity (*see* Smith and Schafer 1984) and coincidence. We are prepared to accept the observed distributions at face value, and consequently we assume that a steady state is operative.

Neglect of advection is possible if $wL/D_B < 1$, where L is the mixing depth. We have no independent estimates of burial velocity, w, except at Sta. 4; there, Fehr (1991) quoted an AMS ^{14}C date of 5,245 yr B.P. at 185 cm, or $w = 0.035$ cm yr^{-1}. As D_B values are likely to be in the range of 0.1–1 cm^2 yr^{-1}, $wL/D_B < 1$ may not always be true. On the other hand, this error will apply equally to each model and should not affect our comparative study.

The solution to the steady-state constant-porosity model is then

Table 2. Best fits of Eq. 10 to the solid volume fraction, $\varphi_s = 1 - \varphi(x)$, at the various Canadian JGOFS sites.

Sta.	Sampling time	$\varphi_s(\infty)$ / $\varphi_s(0)$	$\varphi_s(\infty)$	α (cm^{-1})	R^2
1	Winter 93	0.091	0.192	0.175	0.98
1	Summer 94	0.144	0.186	0.211	0.95
2	Winter 93	0.105	0.203	0.199	0.98
2	Summer 94	0.133	0.207	0.268	0.88
3	Winter 93	0.111	0.177	0.184	0.99
3	Summer 94	0.116	0.166	0.122	0.98
4	Summer 93	0.150	0.244	0.177	0.91
4	Winter 93	0.165	0.248	0.113	0.99
4	Summer 94	0.168	0.236	0.154	0.99
5	Summer 93	0.194	0.327	0.577	0.96
5	Summer 94	0.116	0.167	0.122	0.99

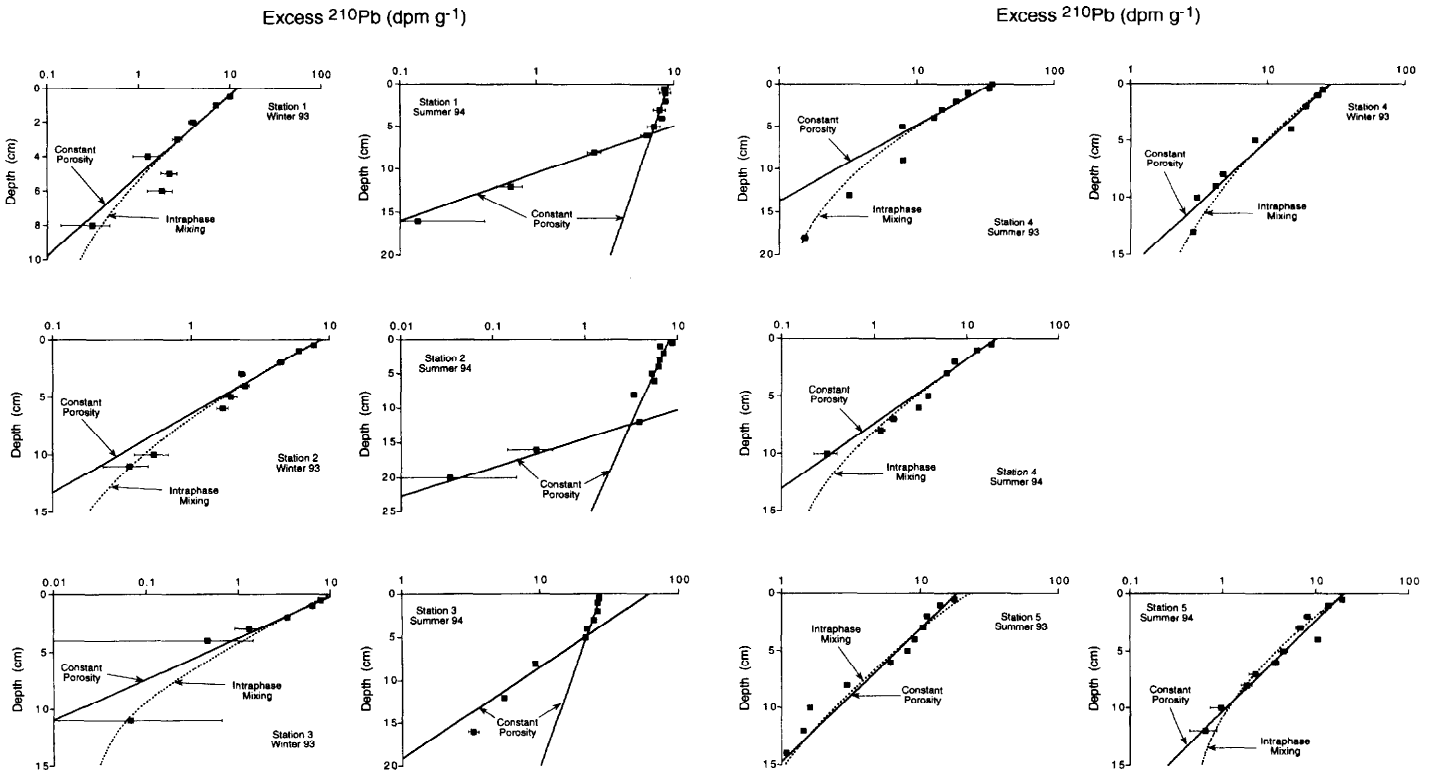

Fig. 4. Plots of excess ^{210}Pb activity with depth in the upper few decimeters of sediments collected at the stations illustrated in Fig. 2 during three cruises. The solid lines are best fits with the constant porosity model, and the corresponding parameters values can be found in Table 3. The dashed lines are best fits with the intraphase mixing model, and the corresponding parameters values can also be found in Table 5. (Note that profiles with two mixing zones were not treated with this latter model.)

$$B(x) = A_1 e^{-ax} + A_2 e^{ax}, \tag{11}$$

where $a \equiv \sqrt{\lambda/D_B}$, A_1 and A_2 are integration constants, and $\lambda = 0.0315$ yr^{-1}. For sites with one mixed zone, i.e. all but Sta. 1, 2, and 3 in summer 1994, the second term in Eq. 11 contributes little to the solution and can be ignored in the fitting process. Even for the two layer sites, i.e. Sta. 1, 2, and 3 in summer 1994, the second term contributes little in each zone except in the immediate vicinity of the interface between the two zones, and, effectively, it can be ignored.

Equation 11, with $A_2 = 0$, was fit to our data via a nonlinear least-squares method. The traditional log-transform approach was not used because it increases the relative importance of the smaller values that also have larger relative errors. The resulting nonlinear fits are displayed in Fig. 4 and tabulated in Table 3. From these results, the constant porosity model does a respectable job of explaining the observed data. Even for the worse case (i.e. Sta. 1 in summer 1994), >80% of the variance is explained by the model.

Now returning to our assumption of steady state, Einstein's relationship, $L^2 = 2D_B t$, tells us the time, t, necessary to obtain a linear steady-state profile from an increase in mixing, i.e. the faster mixed zones at Sta. 1, 2 and 3 in the summer of 1994. By using the greatest D_B value of 12 cm^2 yr^{-1} and a mixed zone of 10 cm, the time necessary to produce this linear profile is >10 yr; therefore, the near-surface changes are not seasonal variations. Greater values of D_B would be inconsistent with the limits imposed by the large dataset presented in Boudreau (1994).

The solution to the steady-state interphase mixing model is

$$B^*(x) = A_1 e^{-ax} + A_2 e^{ax}, \tag{12}$$

where $a \equiv \sqrt{\lambda/D_B^*}$ this time, and A_1 and A_2 are again integration constants. The second term in Eq. 12 was also ignored in this case. Best fits of this model are illustrated in Fig. 5, which are log-linear plots of $B^* = (1 - \varphi)B$.

Some qualitative differences with the results in Fig. 4 are apparent. The more intensely mixed surficial zones at Sta. 1 and 2 in summer 1994 have become completely well mixed on the timescale of ^{210}Pb decay. In addition, new more intensely mixed surface zones have appeared at Sta. 4 in winter 1993 and Sta. 5 in summer 1993. When the effects of porosity gradients are accounted for at these latter stations, the level of mixing is predicted to be much greater than in the constant porosity interpretation.

Best-fit values of D_B^* (with 1σ errors) and corresponding R^2 values are provided in Table 4. The infinite values of D_B^* are not necessarily that large, but appear so on the timescale for ^{210}Pb decay. Some of the R^2 values in Table 4 are relatively low, i.e. <0.8, but these also correspond to the intensely mixed zones at Sta. 4 in winter 1993 and Sta. 5 in summer 1993. Fitting a line to such weak slopes and few data points is a recipe for low R^2 values, which does not

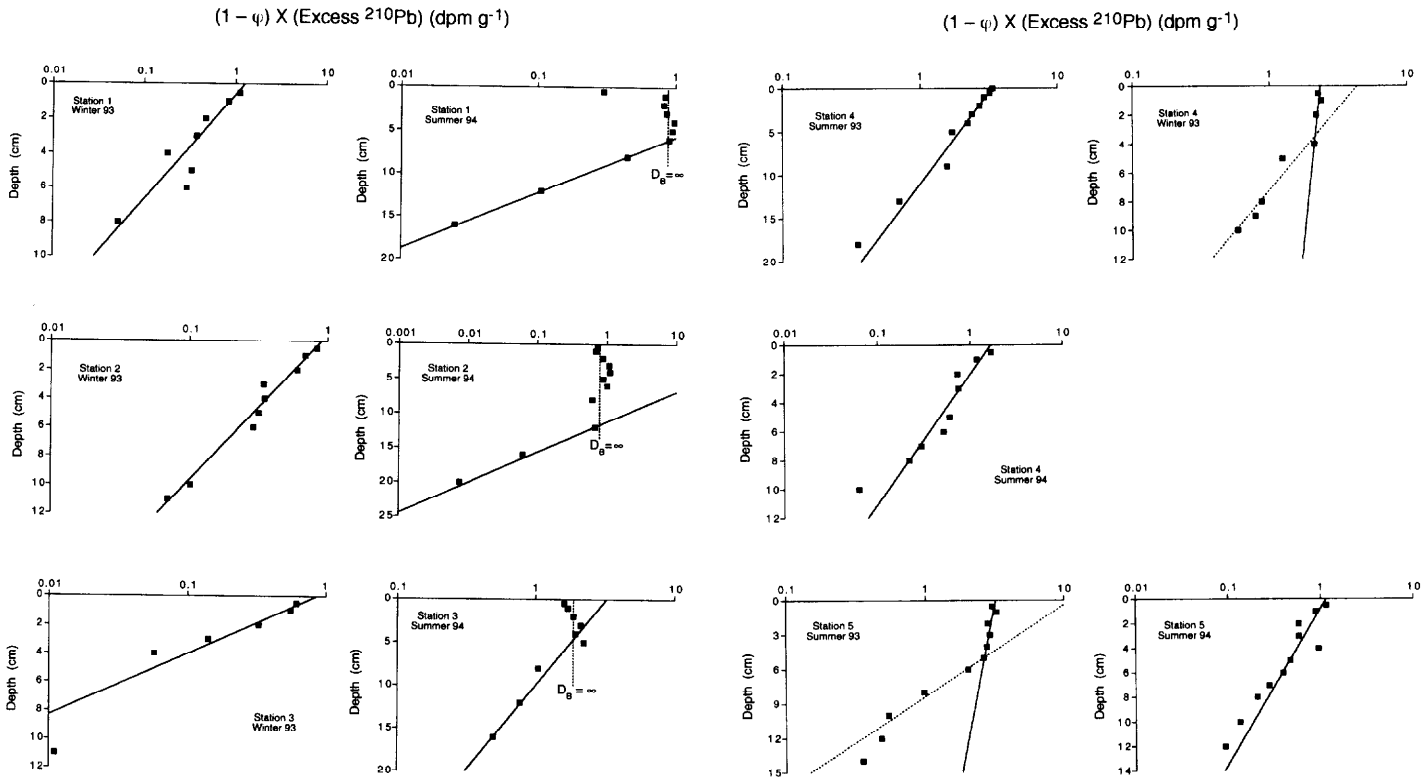

Fig. 5. Plots of the product of the solid volume fraction, $1 - \varphi$, and the excess ^{210}Pb activity with depth in the upper few decimeters of sediments collected at the stations illustrated in Fig. 2 during three cruises. The solid lines are best fits with the interphase mixing model, and the corresponding parameters values can be found in Table 4.

really reflect the ability of the model to explain the data. Otherwise, the R^2 values are comparable to the values assuming constant porosity.

Why do these well-mixed zones appear with interphase mixing? In large part, this is simply the effect of multiplying the increasing function $1 - \varphi(x)$ with the decreasing ^{210}Pb activity, which creates a quantity $(1 - \varphi)B$ that is roughly constant over the first 10 or so cm; nevertheless, the resulting interpretation is that mixing is intense. Surface well-mixed zones develop because of the particular mode, density, and depth distribution of bioturbating organisms and because of physical effects, such as wave mixing. The latter is quite unlikely at our stations. Wave mixing would likely be purely interphase mixing.

Table 3. Calculated biodiffusion coefficients, D_B (±1 SD), for the constant porosity model obtained by nonlinear least-squares fitting of the $^{210}Pb_{ex}$ data.

Sta.	Sampling time	Depth range (cm)	D_B (cm^2 yr^{-1})	R^2
1	Winter 93	0–10	0.13±0.04	0.95
1	Summer 94	0–6	13.2±6.1	0.80
1	Summer 94	6–15	0.18±0.02	0.99
2	Winter 93	0–12	0.28±0.05	0.97
2	Summer 94	0–14	5.1±2.0	0.82
2	Summer 94	14–21	0.08±0.002	1.0*
3	Winter 93	0–12	0.08±0.01	0.99
3	Summer 94	0–5	12.1±6.2	0.84
3	Summer 94	5–16	0.68±0.23	0.97
4	Summer 93	0–18	0.47±0.11	0.96
4	Winter 93	0–13	0.72±0.11	0.98
4	Summer 94	0–11	0.19±0.04	0.97
5	Summer 93	0–15	0.81±0.13	0.97
5	Summer 94	0–12	0.37±0.12	0.89

* Alternatively, w = 0.053 cm yr^{-1}.

The upper sensitivity limit of ^{210}Pb to D_B* values is at most 100 cm yr^{-1}. If this value is put into Einstein's relationship, then the corresponding response time for a 10-cm ^{210}Pb profile falls to 0.5 yr; therefore, it might be implied that the changes at Sta. 1, 2 and 3 could be seasonal. This deduction would be incorrect because the winter profile must be reestablished with a smaller mixing coefficient value, and that is not possible.

The results of fitting the intraphase mixing model are also illustrated in Fig. 4. The model equation that is fit is

$$D_B \bullet \frac{d}{dx}\left[\varphi_s(x)\frac{dB}{dx}\right] - \lambda\varphi_s(x)B = 0, \qquad (13)$$

where $\varphi_s(x)$ is provided by Eq. 10. This equation has no usable analytical solution with Eq. 10 for φ_s. A numerical solution was obtained by finite-difference approximation (Boudreau 1986). The solution was optimized for D_B, i.e. fit to the data, using a Minpack routine. (Fitting was not pos-

Table 4. Calculated biodiffusion coefficients, D_B* (±1 SD), for the interphase mixing model and using nonlinear least-squares fitting of the $^{210}Pb_{ex}$ data.

Sta.	Sampling time	Depth range (cm)	D_B* (cm^2 yr^{-1})	R^2
1	Winter 93	0–8	0.22±0.076	0.91
1	Summer 94	0–6	∞	
1	Summer 94	6–15	0.25±0.032	0.99
2	Winter 93	0–12	0.61±0.12	0.96
2	Summer 94	0–14	∞	
2	Summer 94	14–21	0.12±0.028	0.99
3	Winter 93	0–12	0.11±0.030	0.97
3	Summer 94	0–5	∞	
3	Summer 94	5–16	2.29±1.01	0.91
4	Summer 93	0–18	2.58±0.39	0.98
4	Winter 93	0–5	47.3±52.2	0.63*
4	Winter 93	5–11	0.76±0.34	0.89
4	Summer 94	0–11	0.48±0.16	0.91
5	Summer 93	0–6	22.2±14.0	0.72
5	Summer 93	6–15	0.37±0.07	0.98
5	Summer 94	0–12	0.95±0.40	0.81

* Profile is essentially vertical, $D_B = \infty$.

Table 6. Statistical comparison of the mixing coefficients predicted by the constant porosity mixing (CPM), intraphase mixing (IAM), and interphase mixing (IEM).

Sta.	Sampling time	Depth range (cm)	Statistical equalities*
1	Winter 93	0–10	CPM = IAM = IEM
1	Summer 94	0–6	CPM ≠ IEM (?)
1	Summer 94	6–15	CPM = IEM
2	Winter 93	0–12	CPM = IAM = IEM
2	Summer 94	0–14	CPM ≠ IEM
2	Summer 94	14–21	CPM = IEM
3	Winter 93	0–12	CPM = IAM = IEM
3	Summer 94	0–5	CPM ≠ IEM (?)
3	Summer 94	5–16	CPM = IEM
4	Summer 93	0–18	CPM = IAM ≠ IEM
4	Winter 93	0–13	CPM = IAM ≠ IEM†
4	Summer 94	0–11	CPM = IAM = IEM
5	Summer 93	0–15	CPM = IAM ≠ IEM‡
5	Summer 94	0–12	CPM = IAM = IEM

* Equality means 95% chance they are similar; (?) indicates that the IEA model has infinitely fast mixing on ^{210}Pb timescale.
† Agreement below 5 cm.
‡ Agreement below 6 cm.

sible for the stations with well-mixed surface layers because of problems with adapting the optimization technique.) The results are curves even on a log-linear plot, and the best-fit D_B values with 1σ errors are presented in Table 5. Unfortunately, the Minpack routine did not return R^2 values. Visually, however, the fits seem to be of the same quality as with the other two models, if not better in some cases.

Finally, the results of a formal statistical comparison of the D_B values obtained from the three models are presented in Table 6. Statistical equality was established by determining if the best-fit values overlapped within twice their respective 1σ confidence intervals. The models were generally in agreement, except for the surficial well-mixed zones at Sta. 1, 2, 3, and 4 in winter 1993 and Sta. 5 in summer 1993 (45% of the stations). Again, the D_B values are predicted to be much higher at those times and stations with interphase mixing. Unfortunately, the data and analyses presented above cannot, in themselves, tell us whether interphase or intraphase mixing, or a combination, occurs at our study sites. It seems that only in situ observations or microcosm experiments will be able to shed light on that question.

Table 5. Calculated biodiffusion coefficients, D_B*, for the intraphase mixing model derived from nonlinear least-squares fitting of the $^{210}Pb_{ex}$ data.

Sta.	Sampling time	Depth range (cm)	D_B*(cm^2 yr^{-1})
1	Winter 93	0–8	0.15±0.020
2	Winter 93	0–12	0.37±0.034
3	Winter 93	0–12	0.12±0.020
4	Summer 93	0–18	0.67±0.094
4	Winter 93	0–13	0.89±0.095
4	Summer 94	0–11	0.24±0.031
5	Summer 93	0–15	0.63±0.091
5	Summer 94	0–12	0.35±0.047

Conclusions

Tracers of sediment mixing, such as excess ^{210}Pb, decay in the upper part of sediments, which also corresponds to the zone of the largest changes in solid volume fraction. Use of so-called mass-depth units in order to deal with bioturbation in the presence of such porosity gradients may be neither correct nor helpful.

We used two end-member models to define the spectrum of possible interactions (modes) between bioturbation and porosity, i.e. interphase or intraphase mixing (Boudreau 1986). A statistical analysis of ^{210}Pb profiles from the east coast of Canada proved that both models are equally capable of explaining this data (i.e. similar R^2 values), as is a model that assumes constant porosity. These models produced statistically equivalent D_B values in 55% of our profiles; for these profiles, this agreement indicated that the constant-porosity model may be adopted, without any particular sacrifice of accuracy in calculating D_B values. In the remaining 45% of the profiles, the interphase mixing model predicted the presence of well-mixed zones in the top 5–15 cm, phenomena not predicted by the other two models. The percentage of cases that disagreed is sufficiently great that we need to obtain additional in situ or experimental evidence to identify the actual mixing modes.

References

ALLER, R. C., L. K. BENNINGER, AND J. K. COCHRAN. 1980. Tracking particle-associated processes in nearshore environments by use of $^{234}Th/^{238}U$ disequilibrium. Earth Planet. Sci. Lett. **47:** 161–175.

ANDREWS, D., AND B. T. HARGRAVE. 1984. Close interval sampling of interstitial silicate and porosity in marine sediments. Geochim. Cosmochim. Acta **48:** 711–722.

ARCHER, D., S. EMERSON, AND C. REIMERS. 1989. Dissolution of calcite in deep-sea sediments: pH and O_2 microelectrode results. Geochim. Cosmochim. Acta **53:** 2831–2845.

BERNER, R. A. 1980. Early diagenesis: A theoretical approach. Princeton.

BOUDREAU, B. P. 1986. Mathematics of tracer mixing in sediments: I. Spatially dependent, diffusive mixing. Am. J. Sci. **286:** 161–198.

———. 1994. Is burial velocity a master parameter for bioturbation? Geochim. Cosmochim. Acta **58:** 1243–1249.

CHRISTENSEN, E. R. 1982. A model for radionuclides in sediments influenced by mixing and compaction. J. Geophys. Res. **87:** 566–572.

———. 1983. Mixing, sedimentation rates and age dating for sediment cores—comment. Mar. Geol. **52:** 291–292.

COCHRAN, J. K. 1985. Particle mixing rates in sediments of the eastern equatorial Pacific: Evidence from ^{210}Pb, ^{239,240}Pu and ^{137}Cs distributions at MANOP sites. Geochim. Cosmochim. Acta **49:** 1195–1210.

FEHR, S. D. 1991. A geoacoustical model for the upper sediments of Emerald Basin. Ph.D. thesis, Dalhousie Univ.

GUINASSO, N. L., JR., AND D. R. SCHINK. 1975. Quantitative estimates of biological mixing rates in abyssal sediments. J. Geophys. Res. **80:** 3032–3043.

IVERSEN, N., AND B. B. JØRGENSEN. 1993. Diffusion coefficients of sulfate and methane in marine sediments: Influence of porosity. Geochim. Cosmochim. Acta **57:** 571–578.

KEEN, M. J., B. D. LONCAREVIC, AND G. N. EWING. 1971. Continental margin of Eastern Canada: Georges Bank to Kane Basin, p. 251–291. *In* A. E. Maxwell [ed.], The sea. V. 4, pt. II. John Wiley and Sons.

KRISHNASWAMI, S., L. K. BENNINGER, R. C. ALLER, AND K. L. VON DAMM. 1980. Atmospherically derived radionuclides as tracers of sediment mixing and accumulation in near-shore marine and lake sediments: Evidence from ^{7}Be, ^{210}Pb and ^{239,240}Pu. Earth Planet. Sci. Lett. **47:** 307–318.

MATHIEU, G., P. E. BISCAYE, AND R. A. LUPTON. 1988. System for measurement of ^{222}Rn at low levels in natural waters. Health Physics **55:** 989–992.

MCCALL, P. L., AND M. J. S. TEVESZ. 1982. The effects of benthos on physical properties of freshwater sediments, p. 105–176. *In* P. L. McCall and M. J. S. Tevesz [eds.], Animal–sediment relations. Plenum.

NOZAKI, Y., J. K. COCHRAN, K. K. TUREKIAN, AND G. KELLER. 1977. Radiocarbon and ^{210}Pb distribution in submersible-taken deep-sea cores from Project FAMOUS. Earth Planet. Sci. Lett. **34:** 167–173.

OFFICER, C. B., AND D. R. LYNCH. 1982. Interpretation procedures for the determination of sediment parameters from time-dependent flux inputs. Earth Planet. Sci. Lett. **61:** 55–62.

———. 1983. Mixing, sedimentation rates and age dating for sediment cores—reply I. Mar. Geol. **52:** 292–296.

RHOADS, D. C. 1974. Organism–sediment relations on the muddy sea floor. Oceanogr. Mar. Biol. Ann. Rev. **12:** 263–300.

———, AND L. F. BOYER. 1982. The effects of marine benthos on physical properties of sediments: A successional perspective, p. 3–52. *In* P. L. McCall and M. J. S. Tevesz [eds.], Animal–sediment relations. Plenum.

SMITH, J. N., AND C. T. SCHAFER. 1984. Bioturbation processes in continental slope and rise sediments delineated by Pb-210, microfossil and textural indicators. J. Mar. Res. **42:** 1117–1145.

Received: 5 September 1996
Accepted: 14 May 1997